Symposium on Thermoacoustics in Combustion: Industry meets Academia (SoTiC 2025)
Sept. 8 - Sept. 11, 2025
Trondheim, Norway
Paper No.: 52

Thermoacoustic FEM modeling of partly autoignition and propagation-stabilized flames

Simon M. Heinzmann[1,2] , Nino A. Leder[1], Harish S. Gopalakrishnan[1] and Mirko R. Bothien[1,3]

Abstract

This paper describes a methodology to thermoacoustically account for different flame types in a single Finite-Element-computation. To do so, the flame segmentation mechanism presented in previous studies is used to characterize the different flame zones. Differentiation is done between propagation-stabilized shear-layer flames and autoignition flames that respond to acoustic perturbations very differently. While autoignition flames mainly respond to acoustic pressure and temperature fluctuations, propagation-stabilized flames respond to acoustic velocity perturbations. Thus, flame transfer functions specific to each flame type are analytically implemented within the frequency domain Finite-Element-computation. Using the novel framework, it is shown that the global FTF obtained from Computational-Fluid-Dynamics (CFD) simulations of a backward facing step reheat combustor can be reproduced accurately in the low-frequency regime for an operating point where the flame is forced in a planar manner. The investigated operating point operates on hydrogen fully premixed at lean and autoignitive conditions. The autoignition framework is validated by comparison to one-dimensional direct-numerical-simulation (DNS). The time averaged CFD heat release rate result is validated with large eddy simulation (LES) data.

Keywords

thermoacoustic, autoignition,reheat-combustor, FEM

Novelty and Significance Statement

The novelty of this work lies in the incorporation of two different types of flame in a single thermoacoustic FEM calculation. To the best of our knowledge, this has not yet been shown in the literature before. The significance of this work lies within industrial applications. In industrial reheat combustion chambers, the autoignition flame is typically not purely autoignition stabilized, and flame anchoring regions are present which contribute to the stability of the flame.

Nomenclature

Abbreviations

PV	Progress Variable
CFD	Computational Fluid Dynamics
CFL	Courant-Friedrichs-Lewy
FEM	Finite-Element-Method
FTF	Flame Transfer Function
HRR	Heat Release Rate
LES	Large eddy simulation
RANS	Reynolds Averaged Navier-Stokes

Greek

$\bar{\dot{\omega}}_{PV}$	Averaged turbulent source term of PV
$\dot{\omega}_{PV}$	Source term of PV
γ	Ratio of specific heats
ω	Angular frequency in rad/s
ρ	Density
σ	Spread of time delay
$\sigma_{\dot{q},ai}$	HRR width of autoignition flame
$\sigma_{\dot{q},ps}$	HRR width of propagation-stabilized flame
τ	Time delay
$Y_{i,0}$	Initial mixture composition

Roman

$(\cdot)'$	Perturbation in time domain
$(\cdot)_0$	Time-averaged quantity
$(\cdot)_{\text{init}}$	Initial
$(\cdot)_{ai}$	Autoignition
$(\cdot)_{ps}$	Propagation-stabilized
$\dot{q}$	Instantaneous total HRR
$\dot{q}_{0,a,ai}$	Volumetric HRR integrated along the streamwise direction of the autoignition flame $[W/m^2]$
$\dot{q}_{0,a,ps}$	Volumetric HRR integrated along the streamwise direction of the propagation-stabilized flame $[W/m^2]$
$\hat{(\cdot)}$	Fourier transform of a fluctuating quantity
$\hat{\dot{q}}$	Volumetric HRR perturbation of entire combustion chamber
$\hat{\dot{q}}_{a,ai}$	Autoignition flame integrated HRR perturbation

[1]ZHAW Zurich University of Applied Sciences, Institute of Energy Systems and Fluid-Engineering, Winterthur, Switzerland
[2]ETH Zürich, Department of Mechanical and Process Engineering, Zürich
[3]Department of Energy and Process Engineering, NTNU, Norway

Corresponding author:
S. M. Heinzmann, ZHAW Zurich University of Applied Sciences, Institute of Energy Systems and Fluid-Engineering, Winterthur, Switzerland
Email: simon.heinzmann@zhaw.ch

$\hat{q}_{a,ps}$	Propagation-stabilized flame integrated HRR perturbation
$\hat{f}_1$	Downstream traveling acoustic wave
$\hat{g}_1$	Upstream traveling acoustic wave
$\hat{h}_1$	Entropic wave
$\hat{x}_{ig}$	Autoignition flame movement perturbation
c_0	Speed of sound
$F1, F2, F3$	Autoignition flame HRR FTFs
f_i	Mass fractions e.g. fuel, hot gas, carrier air
FTF_{ps}	Propagation-stabilized flame HRR FTF
$G1, G2, G3$	Autoignition flame movement FTFs
p	Pressure
$P(\cdot)$	Probability
p_{op}	Operating pressure
p_{ref}	Pressure at reference location
T	Temperature
t	Time
u	Velocity
x, y, z	x-,y- and z-coordinates
$x_{ig,0}$	Mean ignition length

Introduction

To fulfill the Paris agreement (1), a large-scale integration of renewable energy systems in the energy landscape is essential (2–4). To stabilize and balance the grid, gas turbines running on carbon-free fuels can be an ideal asset (3; 5–9). However, these non-conventional fuels possess very different combustion properties when compared to natural gas. Thus, novel gas turbine combustor development is faced with new challenges to enable the fuel flexible firing capability of an engine. The thermoacoustic analysis to aid the mitigation of combustion instabilities remains a key component in the development phase (10).

There are a variety of methods to perform thermoacoustic analysis of combustion chambers. Direct numerical simulation (DNS) (11; 12) and large eddy simulation (LES) (13) are considered high-fidelity analysis tools, which are capable of analyzing certain thermoacoustic effects in the highest detail. However, they come with a high computational cost and are unfeasible for entire industrial combustor geometries. Alternatively, Helmholtz solvers in combination with flame transfer/describing functions extracted from computations or experiments have been shown to accurately capture the thermoacoustics of combustion chambers (14–20). Nicoud et al. (14) showed that using a FEM Helmholtz solver the stability of combustion chambers with propagation-stabilized flames could be captured accurately. To do so, the flame transfer function (FTF) was described by an $n-\tau$ model (21). Laera et al. (15) also used a Helmholtz solver together with a flame describing function to correctly capture the stability of a laboratory scale annular combustion chamber comprised of multiple matrix burners. Silva et al. (19) combined a Helmholtz solver with a flame describing function for a swirl-stabilized combustion chamber to predict the acoustic pressure amplitudes of limit-cycles. Generally, the application of Helmholtz solvers to perform thermoacoustic analysis significantly reduces computational time compared to DNS and LES. Alternatively, network-models have shown to be able to reproduce the combustion chamber acoustics and flame interaction with the highest computational efficiency (22–26).

In this paper, we present an FEM based approach to thermoacoustically model flames that are partly stabilized by autoignition. The overall flame, which consists of a propagation- and an autoignition part, is analytically described in FEM. The segmentation mechanism from prior studies (17; 18) is leveraged to define the different flame types. The segmentation mechanism (17; 27) was initially designed to thermoacoustically model non-compact reheat flames under the influence of transverse combustor eigenmodes. In the case of transverse eigenmodes, the acoustic wavelength is of similar length as the flame, thus, resulting in an acoustically non-compact flame. To deal with this, the segmentation mechanism divides the flame into multiple subflames in transverse direction. Each of the very thin subflames is then considered acoustically compact without variation of the fluctuation quantities across its height. Thus, single values for the pressure, temperature and velocity fluctuations act on each subflame. For each of the subflames, a transfer function can be assigned. In the study presented here, the flame is acoustically compact and as such no segmentation is needed. However, the segmentation mechanism is leveraged to assign a specific FTF to each heat release rate (HRR) region depending on its flame stabilization type. To obtain the flame characterization parameters, RANS simulations are done using Fluent with an in-house reheat flame model, which is an adaptation and extension of the model derived by Kulkarni et al. (28; 29). The thermoacoustic analysis is done for a planarly forced backward facing step (BFS) burning hydrogen at elevated pressure.

The presented research is relevant, because in industrial reheat combustors the autoignition flame is never only stabilized by autoignition. Typically, the reheat flame consists of propagation-stabilized HRR regions as well as regions predominantly stabilized by autoignition. Propagation-stabilized flames occur within the shear layers of recirculation zones. Their stabilization is governed by the balance of the flame consumption speed and the flow velocity. With respect to thermoacoustics, the acoustic waves affect the propagation-stabilized flame regions by velocity fluctuations, which modulate the equivalence ratio. In contrast, autoignition stabilized flames are governed by the balance of the autoignition time scale and the flow residence time scale. The fluctuating pressure and especially the isentropic temperature fluctuations induced by acoustic waves affect the local reaction rates and thus the ignition chemistry. This can strongly alter the ignition time and therefore the ignition length, which results in HRR fluctuations. Thereby, the history effect of the fluctuations during the ignition phase matters for reheat flames and is accounted for in current state-of-the-art flame response modeling tools, as presented in Refs. (17; 27; 30–33).

Validation data

The segmentation mechanism developed by Heinzmann et al. (17; 18) was already validated in prior studies and initially designed to numerically deal with acoustically non-compact flames. This segmentation mechanism can also be efficiently used for the planar wave case to incorporate different flame types. The model is compared to 1D DNS (32) for a flame solely stabilized by autoignition, and to RANS computations for the partly autoignition- and propagation-stabilized flame in a BFS combustion chamber.

1D DNS simulation

The CFD study used for validation in Ref. (34) is a compressible 1D DNS computation burning hydrogen fully premixed at lean conditions. The operating pressure is atmospheric with an inlet temperature of 1100 K and an inlet flow speed of 200 m/s. The duct of length 0.3 m with non-reflecting boundary conditions was forced with acoustic and entropic waves at the inlet. For more details on the numerical setup the reader is referred to Ref. (34). The duct is modeled in 2D in FEM with a length of 0.3 m and a height of 0.05 m. The boundary conditions were set to non-reflecting and the $\hat{f}_1$ and $\hat{g}_1$ acoustic forcing state from the CFD initialized by forcing with $\hat{f}_{1,b}$, $\hat{h}_{1,b}$ and $\hat{g}_{2,b}$ waves (Fig. 1), where the subscript b stands for boundary. Because the Helmholtz equation does not account for any mean flow effects, entropic waves incident at the inlet were forced directly within the mathematical flame formulation via a harmonic source term.

Autoignition flame RANS computation

The 2D RANS CFD computations are performed for a BFS Fig. 2 with a total length of 0.3 m. The BFS is located at 0.15 m, with a symmetric area expansion from 0.01 m to 0.02 m. The investigated operating point burns hydrogen and air fully premixed at lean and autoignitive conditions (mass fractions: H_2 (0.0053), O_2 (0.1842), H_2O (0.0521), N_2 (0.7584)). The inlet velocity measures 150 m/s, the mean operating pressure is 12.9 bar, and the inlet temperature is 1143 K. The simulation is done using ANSYS Fluent 2024 R1 (35) with an in-house combustion model which is based on the work of Kulkarni et al. (28; 29). In the combustion model, the radical buildup during the induction phase is represented by a normalized progress variable (PV). The PV and its source term is obtained by tracking representative intermediate and product species (here HO_2 and H_2O) in 0D reactors. For normalization, the sum of the tracked species mass fractions is then divided by its sum at equilibrium. It can be shown, that for fully premixed conditions, the PV source term only depends on the temperature, pressure and the current ignition progress (36).

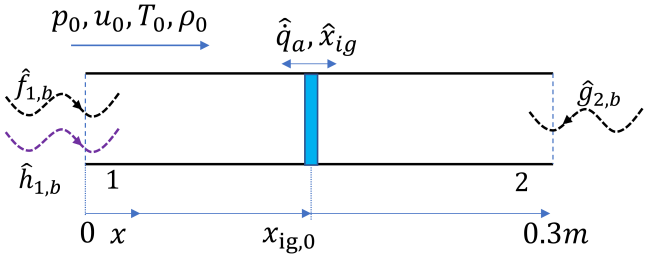

Figure 1. 1D DNS configuration schematic of the modeled duct in the FE-solver. The boundaries are forced with $\hat{f}_{1,b}$, $\hat{h}_{1,b}$ and $\hat{g}_{2,b}$ waves.

$$\dot{\omega}_{\mathrm{PV}} = \dot{\omega}_{\mathrm{PV}}(T, p, PV) \tag{1}$$

Assuming, that the temperature does not change significantly during the radical build up, it can be divided into two parts: The initial temperature $T_{0,init}$ and the fluctuating temperature T' due to the acoustic forcing. Similarly, the pressure is divided into the operating pressure p_{op} and the fluctuating part p'.

$$\dot{\omega}_{\mathrm{PV}} = \dot{\omega}_{\mathrm{PV}}(T_{0,\mathrm{init}}, T', p_{\mathrm{op}}, p', PV) \tag{2}$$

By assuming isentropic correlation of pressure and temperature for acoustic waves, T' can be expressed using p', p_{op} and $T_{0,init}$:

$$T' = T_{0,\mathrm{init}} \left(\frac{p'}{p_{\mathrm{op}}} + 1 \right)^{\frac{\gamma-1}{\gamma}} + T_{0,\mathrm{init}} \tag{3}$$

As p_{op} and $T_{0,init}$ are constant and known $a\ priori$, the PV source term is defined by:

$$\dot{\omega}_{\mathrm{PV}} = \dot{\omega}_{\mathrm{PV}}(p', PV) \tag{4}$$

For the turbulence chemistry interaction (TCI) a presumed beta PDF (37) approach is used. The mean turbulent PV source term is then obtained by folding the source term over a probability distribution $P(PV)$ which is defined by the PV's mean and variance:

$$\bar{\dot{\omega}}_{\mathrm{PV}} = \int_0^1 \dot{\omega}_{\mathrm{PV}}(p', PV)\, P(PV)\, dPV \tag{5}$$

The reaction rate is then computed by multiplying the Eddy Dissipation Model's (38) reaction rate with the value of the PV in order to delay it until the residence time of a fluid particle is equal to the ignition delay time.

The advantage of this approach is that the correct ignition delay time can be achieved without transporting all the intermediate species and computing their reaction rates. Instead, the PV source terms are computed $a\ priori$ using a detailed mechanism (SanDiego (39)) and stored in a lookup table.

For the CFD simulations the realizable $k-\epsilon$ turbulence model and second order temporal and spatial discretization is used with a timestep of 6e-6 s to obtain an acoustic CFL of 0.96. The structured uniform mesh consists of hexahedral elements with a size of 0.5 mm. A mesh independence study has been made comparing element sizes of 0.2 mm and 0.125 mm. The RANS mean field is validated by comparison to data from a compressible LES computation of the same geometry and at the same operating point. The OpenFoam code (40) is used to solve the Navier-Stokes equations. The partially-stirred reactor (PaSR) turbulent combustion model is employed. The LES simulation is setup identically to the shorter BFS shown in Gopalakrishnan et al. (33).

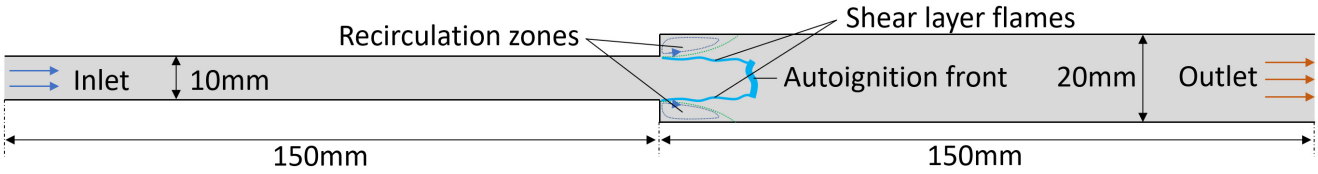

Figure 2. Schematic of the backward facing step (BFS) geometry.

Methodology

Flame response and segmentation

The flame response to planar acoustic waves is characterized differently for the propagation-stabilized shear layer flames and the autoignition flame. For the shear layer flame, an $n-\tau-\sigma$ model is implemented, similarly to (41), using Eq. 6. The FTF thereof (FTF_{ps} Eq. 7) relates the HRR perturbations to the velocity fluctuations at the dump plane, and is derived from the initial $n-\tau$ model from Crocco (21). The magnitude n has been chosen equal to 1 to satisfy the low frequency FTF limit for fully premixed propagation-stabilized flames (gain equal to 1) (42). The second exponential term $exp(-\sigma_{ps}^2\tau_{ps}^2/2)$ is a measure for the delay spread across the flame and acts as a low-pass filter at higher frequencies. They are calculated by fitting Gaussian kernels to the timely averaged HRR field and evaluating the location and spread of ignition lengths.

$$\frac{\hat{\dot{q}}_{a,ps}}{\dot{q}_{0,a,ps}} = exp(i\omega\tau_{ps})exp(-\sigma_{ps}^2\tau_{ps}^2/2)\frac{\hat{u}_x(x_{ref,y})}{\bar{u}_0} \tag{6}$$

$$FTF_{ps} = \frac{\frac{\hat{\dot{q}}_{a,ps}}{\dot{q}_{0,a,ps}}}{\frac{\hat{u}_x(x_{ref,y})}{\bar{u}_0}} \tag{7}$$

For the autoignition flame, the framework from Gopalakrishnan et al. (32) is used to quantify the flame response. The total autoignition HRR response of the flame is assumed to be a linear superposition of the individual flame responses (FTFs) to the acoustic and entropic waves (31). Eq. 8 represents the HRR FTFs $F_i(\omega)$ and Eq. 9 characterizes the flame movement using the $G_i(\omega)$ FTFs. $\hat{\dot{q}}_{a,ai}/\dot{q}_{0,a,ai}$ is the normalized heat release rate perturbation, $\hat{x}_{ig}/x_{ig,0}$ the normalized flame movement, $\dot{q}_{0,a,ai}$ (W/m^2) is the mean heat release rate per unit area and $x_{ig,0}$ the mean ignition length (32). $\hat{f}_1$ is the downstream traveling acoustic wave, $\hat{g}_1$ the upstream traveling acoustic wave and $\hat{h}_1$ the with the flow transported entropic wave (32).

$$\frac{\hat{\dot{q}}_{a,ai}}{\dot{q}_{0,a,ai}} = F_1(\omega)\frac{\hat{f}_1}{p_0} + F_2(\omega)\frac{\hat{g}_1}{p_0} + F_3(\omega)\frac{\hat{h}_1}{p_0} \tag{8}$$

$$\frac{\hat{x}_{ig}}{x_{ig,0}} = G_1(\omega)\frac{\hat{f}_1}{p_0} + G_2(\omega)\frac{\hat{g}_1}{p_0} + G_3(\omega)\frac{\hat{h}_1}{p_0} \tag{9}$$

FEM implementation

To characterize the flame in the FEM simulation and solve the inhomogeneous Helmholtz equation (Helmholtz equation with source terms), the numerical segmentation mechanism derived by (17; 18) is used. A main benefit of the segmentation is, that simulations can be done for non-compact flames, i.e. flames that are under the influence of transverse eigenmodes. Fig. 3 schematically visualizes the segmentation mechanism. Differentiation is made between propagation-stabilized subflames (blue circles) and the autoignition subflames (magenta circles). Due to the fine segmentation, it can be assumed that for each subflame a single value for the pressure and velocity perturbation is present. Thus, the flame also reacts with a single value for the HRR and the flame movement. For each of the subflames, specific FTFs can be implemented to capture the different flame responses of propagation-stabilized and autoignition flames. Hence, the segmentation mechanism allows different flame types in the same FEM computation.

For the propagation-stabilized flame parts (Eq. 10) as well as the autoignition flame regions (Eq. 11), Gaussian kernels are used to analytically position the flame in the computational domain. $\sigma_{\dot{q},ps}$ and $\sigma_{\dot{q},ai}$ are measures for the HRR width, $x_{f,ps}(y)$ and $x_{ig,0}(y)$ the mean flame positions.

$$\dot{q}_{ps}(x,y) = \frac{\dot{q}_{0,a,ps}(y)}{\sigma_{\dot{q},ps}(y)\sqrt{2\pi}}\exp\left(-\frac{1}{2}\left(\frac{x-x_{f,ps}(y)}{\sigma_{\dot{q},ps}(y)}\right)^2\right) \tag{10}$$

$$\dot{q}_{ai}(x,y) = \frac{\dot{q}_{0,a,ai}(y)}{\sigma_{\dot{q},ai}(y)\sqrt{2\pi}}\exp\left(-\frac{1}{2}\left(\frac{x-x_{ig,0}(y)}{\sigma_{\dot{q},ai}(y)}\right)^2\right) \tag{11}$$

The parameters for the HRR width, the mean flame position and the integrated HRR can be calculated from either CFD mean field solutions or experimental chemiluminescence imaging if available. Using these quantities and the assumption of the Gaussian kernel in x-direction (multiple studies used Gaussian distributions (17; 30; 31; 34; 43)), the average flame can be rebuilt fully in FEM. Whilst the procedure here is done in 2D on the xy-plane, the previous study (27) derived the identical procedure in 3D. Hence, the new method shown here can also be used in 3D.

At this point, the average flame is fully characterized in the FEM simulation and what remains to be characterized is the representation of the fluctuating HRR perturbations. This is achieved by obtaining the instantaneous HRR after multiplying the mean HRR by the FTF Eq. 8 (for the propagation-stabilized flame Eq. 6 respectively) and accounting for the flame motion in the Gaussian distribution using Eq. 9 to obtain Eqs. 12. For the propagation-stabilized

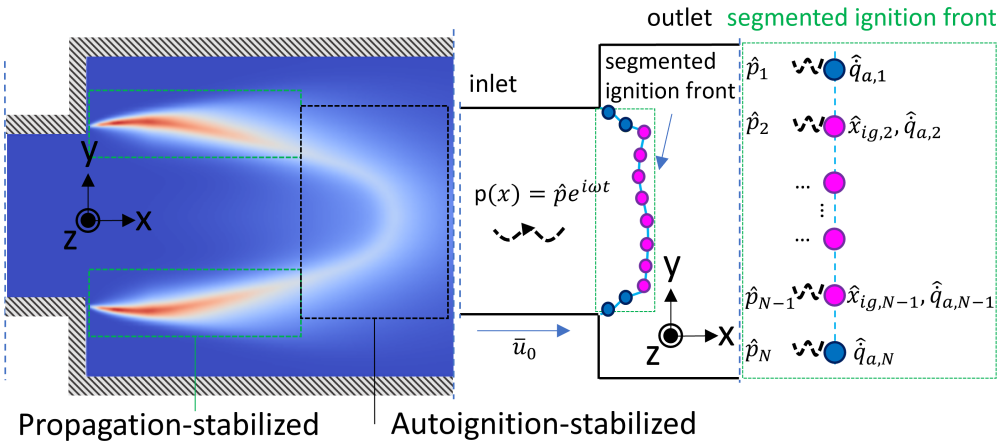

Figure 3. Numerical segmentation method for a perturbed partly autoignition and propagation-stabilized flame in 2D. The blue circles indicate the propagation-stabilized flame parts, and the magenta circles represent the autoignition flame.

flame region, no flame motion is introduced due to the anchored nature of the flame.

$$\begin{aligned}\hat{\dot{q}}_{a,ps}(y) =& \dot{q}_{0,a,ps}(y) FTF_{ps} \frac{\hat{u}_x(x_{ref}, y)}{\bar{u}_0} \\ \hat{\dot{q}}_{a,ai}(y) =& \dot{q}_{0,a,ai}(y) \left(F_1(\omega) \frac{\hat{f}_1}{p_0} + F_2(\omega) \frac{\hat{g}_1}{p_0} + F_3(\omega) \frac{\hat{h}_1}{p_0} \right)\end{aligned} \tag{12}$$

Using Gaussian kernel distributions for both flames the instantaneous volumetric HRR is obtained (Eq. 13).

$$\begin{aligned}\dot{q}(x,y) =& \frac{\dot{q}_{0,a,ps}(y)}{\sigma_{\dot{q},ps}(y)\sqrt{2\pi}} \dots \\ & \exp\left(-\frac{1}{2} \left(\frac{x - x_{f,ps}(y)}{\sigma_{\dot{q}}(y)} \right)^2 \right) \left(\frac{\hat{\dot{q}}_{a,ps}(y)}{\dot{q}_{0,a,ps}(y)} + 1 \right) + \dots \\ & \frac{\dot{q}_{0,a,ai}(y)}{\sigma_{\dot{q},ai}(y)\sqrt{2\pi}} \exp\left(-\frac{1}{2} \left(\frac{x - x_{ig,0}(y) - \hat{x}_{ig}(y)}{\sigma_{\dot{q},ai}(y)} \right)^2 \right) \dots \\ & \left(\frac{\hat{\dot{q}}_{a,ai}(y)}{\dot{q}_{0,a,ai}(y)} + 1 \right)\end{aligned} \tag{13}$$

The fluctuating HRR $\hat{\dot{q}}(x,y)$, which is the source term for the Helmholtz equation, is consequently computed by subtracting the mean HRR from the instantaneous counterpart (Eq. 14).

$$\hat{\dot{q}}(x,y) = \dot{q}(x,y) - (\dot{q}_{ps}(x,y) + \dot{q}_{ai}(x,y)) \tag{14}$$

The equation for the inhomogeneous Helmholtz equation, which is solved in FEM (in the frequency domain), thus becomes Eq. 15 by adding the source term to the right-hand side of the homogeneous Helmholtz equation. From the computations the eigenfrequencies and linear growth rates are extracted. In this study COMSOL 6.2 is used.

$$\nabla \cdot \left(\frac{1}{\rho_0} \nabla \hat{p} \right) + \frac{\omega^2}{\gamma p_0} \hat{p} = -i\omega \frac{\gamma - 1}{\gamma} \hat{\dot{q}}(x,y) \tag{15}$$

Results

Results obtained by implementing the proposed methodology are shown in this following section.

1D DNS forced

Fig. 4 shows the intermediate result obtained in comparison with the DNS simulation to validate the FEM implementation of a flame solely stabilized by autoignition. An excellent match is achieved in comparison with the DNS result in both phase and magnitude. The small deviation in phase could result from neglecting mean flow effects by employing the Helmholtz equation.

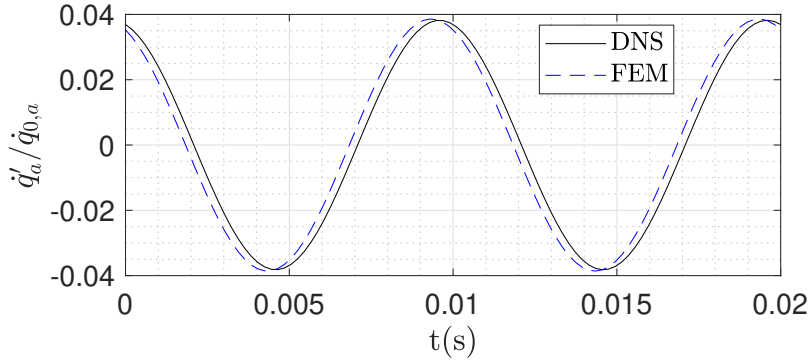

Figure 4. Comparison of the HRR fluctuations for the 1D DNS configuration forced at 100Hz. The solid line represents the DNS data and the dashed line the FEM result.

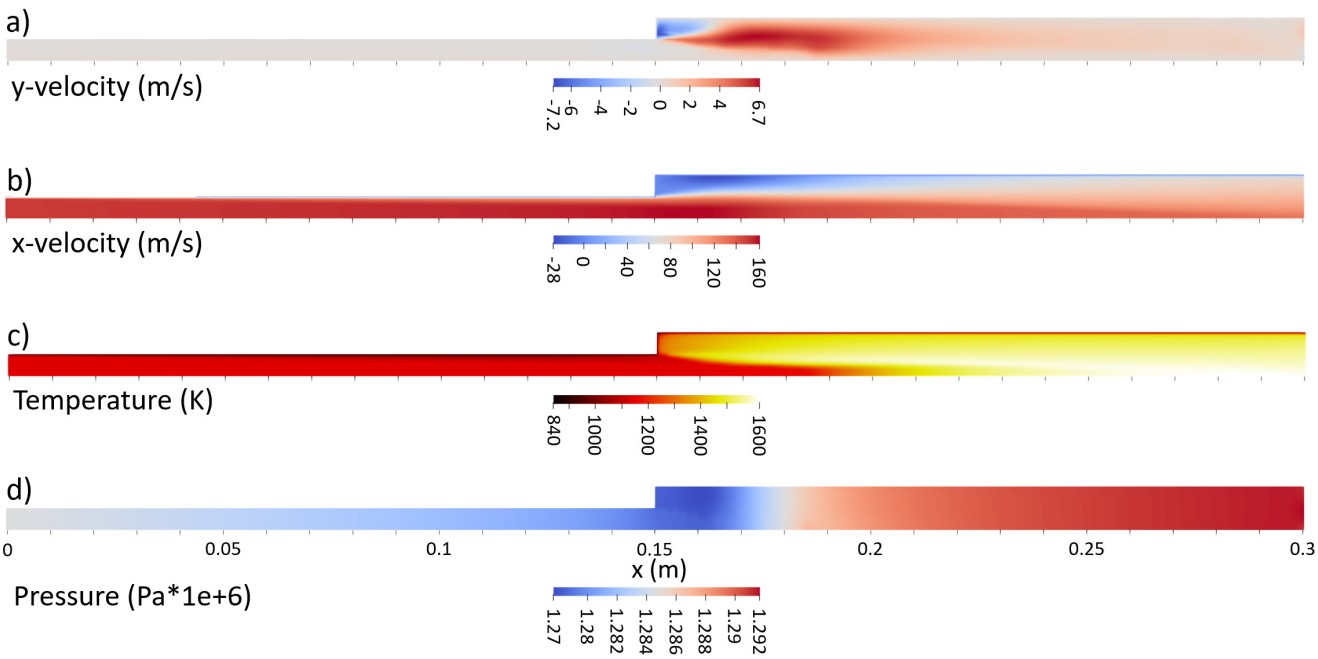

Figure 5. Mean field solutions of the RANS simulation: a) y-velocity, b) x-velocity, c) temperature and d) pressure.

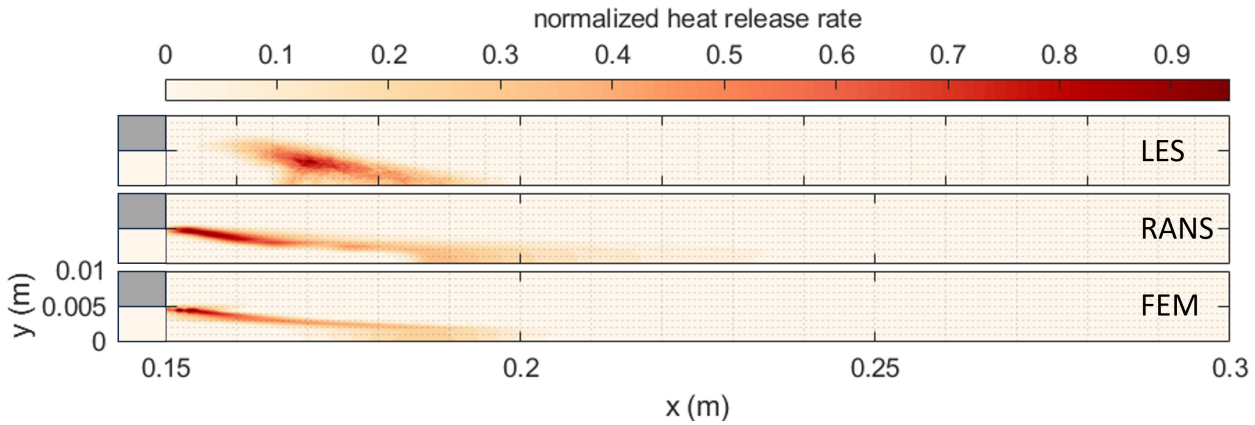

Figure 6. Comparison of the mean HRR between LES (top) RANS (middle) and FEM (bottom). The backward facing step is located at $x = 0.15m$.

Mean fields of the BFS burning hydrogen

Figure 5 shows the time-averaged mean fields from the RANS simulation. Figure 5a) shows the y-velocity. The recirculation zone is visible by the blue and red areas. Figure 5b) displays the x-velocity. The recirculation zone can again be nicely observed by the negative velocity areas in blue. The temperature distribution is given in Fig. 5c) and matches well with the results from CANTERA simulations. Lastly, the pressure is shown in Fig. 5d), where a pressure drop downstream of the area jump is observed and a pressure increase downstream of the flame.

The time-averaged flame shape is computed using the in-house autoignition reheat flame model described in the CFD section. To validate the mean field qualitatively, comparisons to center-plane data from the described LES simulation are made. The comparison between the results from the LES and the RANS simulations shows that the model can replicate the flame to a certain extent. The mean ignition-length and overall flame shape is captured well (length scales are small). The RANS simulation however predicts the propagation-stabilized shear layer flames to be further upstream compared to the validation data. Experience shows, that the occurrence of an earlier timed ignition is linked to the RANS solver used in combination with the reheat flame model.

Further comparisons can be made by analyzing the volumetric HRR of Fig. 6 for two different sections in Fig. 7. The three dash-dotted blue lines show the normalized volumetric HRR along a section ($y = 0.001m$) across the shear layer flame. The diamonds represent the LES data, the circles the RANS data and the stars the FEM data, respectively. As was already indicated before, the HRR peak of the shear layer flame occurs further upstream in the RANS simulation at 0.158m compared to 0.169m. The FEM value matches the one of the RANS closely with 0.157m. The peak value is over-predicted by the RANS compared to the LES simulation. The solid magenta lines provide the same comparison for a section at a y-coordinate of 0.001m, close to the symmetry line. In this region the flame is stabilized by autoignition. The peak of the RANS simulation is at an

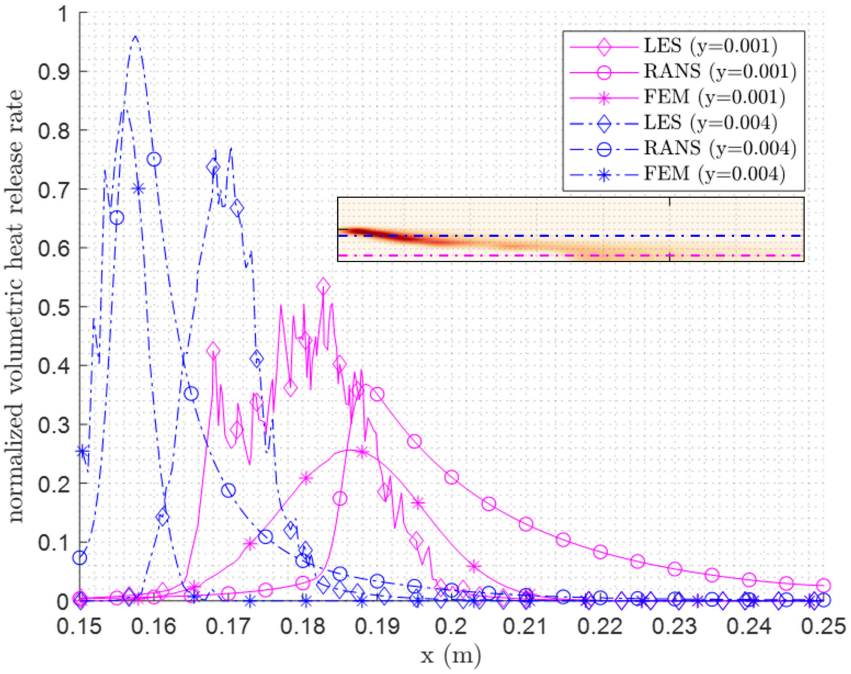

Figure 7. Comparison of the volumetric HRR of different sections through the shear layer flame (blue dash-dotted lines.) and the autoignition stabilized part (solid lines). The comparison is made between the LES (diamonds), RANS (circles) and the FEM (stars).

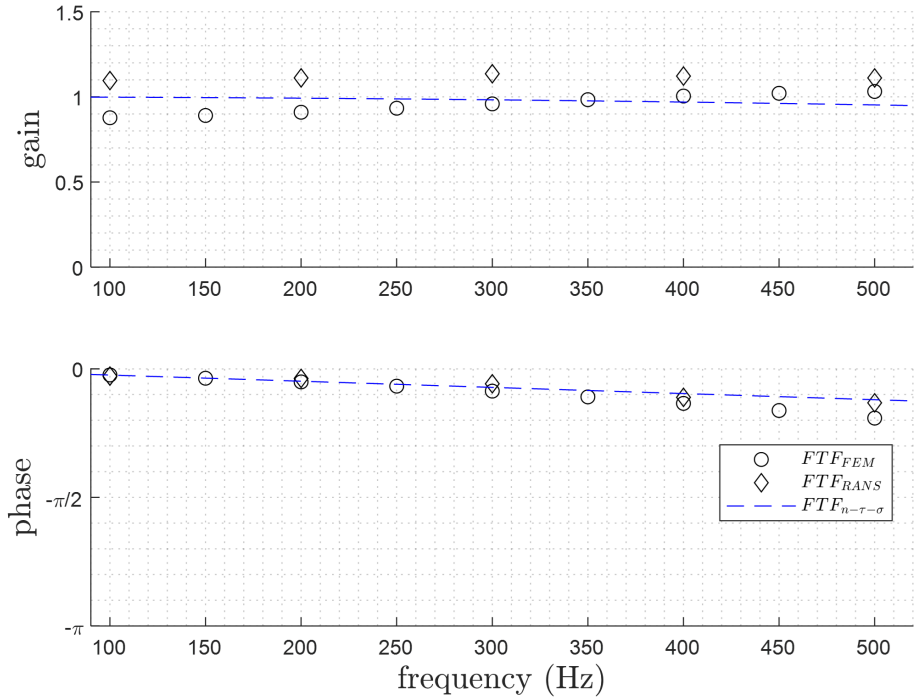

Figure 8. FTF Comparisons between the CFD results (diamonds) and the FEM computation (circles). The blue dashed line represents the used $n - \tau - \sigma$ model.

x-coordinate of 0.188m. It is predicted further downstream compared to the LES at around $\sim$ 0.18m. The mean ignition length of the FEM matches the RANS closely with 0.186m. The HRR distribution is spread more symmetrically around the peak compared to the RANS, which is a prerequisite of the introduced mathematical model (Eq. 13). More generally, the flame appears more compact in the LES compared to the RANS computation. Due to the match of the overall flame shape, the RANS mean field can still be used for the subsequent study. Simulations with harmonic acoustic forcing at the inlet with a pressure amplitude of 0.5% are performed using ANSYS Fluent. The values of the $n - \tau - \sigma$ model are computed to be $n = 1$ (low frequency limit for fully premixed propagation stabilized flames (42)), $\sigma = 0.099ms$ and $\tau = 0.12ms$ using the method described in the methodology section.

The forced FEM simulation is set up identically to the RANS computation by forcing harmonically at the inlet with a pressure amplitude of 0.5%. The outlet is set to

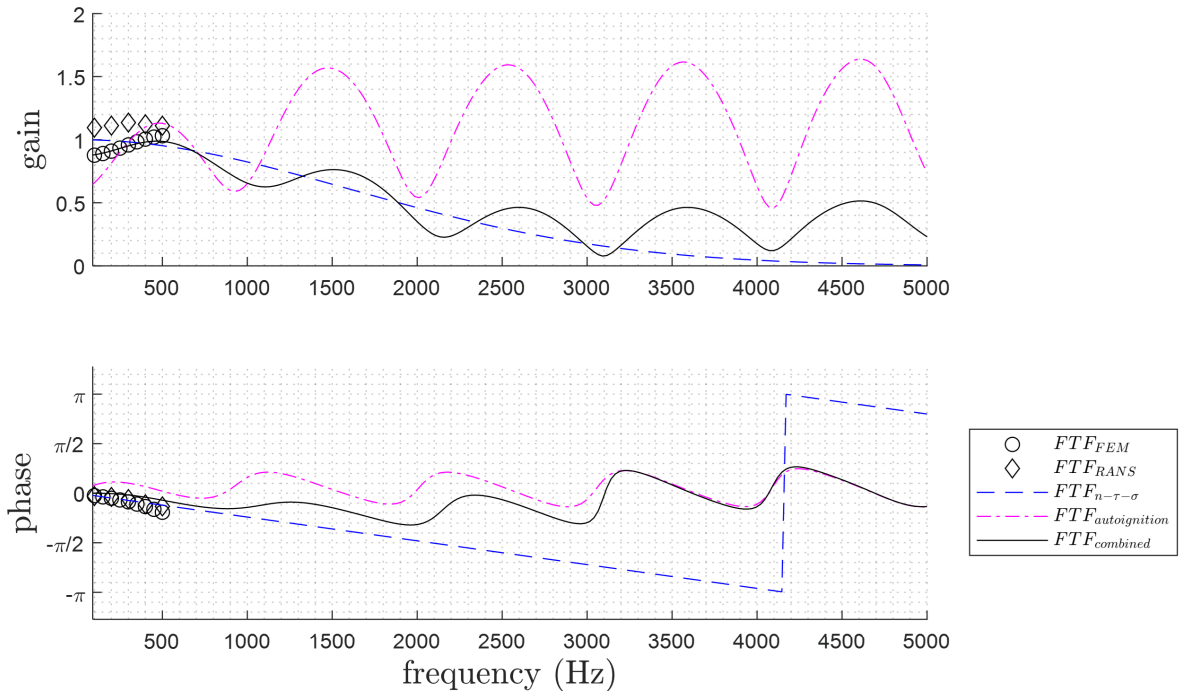

Figure 9. FTF Comparisons between the $n-\tau-\sigma$ model (blue dashed) and the autoignition FTF (magenta dash-dotted line). The solid black line is the combination of both FTFs. The circles represent the FTF from the FEM, and the diamonds the FTF from the RANS simulations.

fully anechoic to mitigate reflections and upstream traveling acoustic g-waves.

Fig. 8 shows the FTFs $(\dot{q}'/\dot{q}_0)/(u'/u_0)$ of both the RANS simulations and the FEM simulations. The FEM computation (circles) is able to capture the phase very accurately. The gain of the FTF shows slight differences between the CFD simulation (diamonds) and the FEM computation. The overall match of the FTF is good, and the newly introduced segmentation model to combine differently behaving reheat flame regions for FEM computations works. Further, the comparison to the dashed blue line, which represents the $n-\tau-\sigma$ model, indicates that the investigated flame response is dominated by the propagation-stabilized flames in the shear layer. Consequently, the proposed methodology can be used in a further step for stability calculations of longitudinal eigenmodes.

For completeness, Fig. 9 shows the used FTFs (with respect to the velocity fluctuations $(\dot{q}'/\dot{q}_0)/(u'/u_0)$) for a larger frequency range. At higher frequencies, the assumption of no mean flow velocity breaks down in the FEM. However, the FTFs can still be analyzed to understand the flame response at higher frequencies. Looking at the $n-\tau-\sigma$ FTF (blue dashed line) of the shear layer flame zones, the low-pass filter behavior can clearly be observed. A negligible HRR response contribution from the shear layer flames from 4000Hz onwards is indicated. The FTF from the solely autoignition stabilized central HRR zone is computed using the Lagrangian framework (32) and is shown by the magenta dash dotted line. The FTF indicates that at higher frequencies the autoignition flame zone contributes to a large extent to the overall flame response. However, no low-pass filter is contained in the model and thus the gain is estimated to be slightly lower in reality. The Lagrangian framework (32) was validated with 1D DNS simulations up to 4000Hz, where deviations of +20% were observed in the gain between DNS and the model. The black solid line represents a superposition of both the shear layer flame FTF and the autoignition flame FTF with an overall autoignition weighting of 0.32 and a shear layer flame weighting of 0.68 respectively. This gives an indication of how the flame behaves globally at higher frequencies, given that the assumption of a superposition of the HRR response of a propagation-stabilized flame region and an autoignition flame region is valid.

Conclusion

With reheat combustors becoming of increasing interest in industrial gas turbines, autoignition flames have shifted into the scope of current research. Especially in industrial reheat combustion chambers, an autoignition flame will likely have certain flame regions that are propagation-stabilized due to either flow recirculation or vortex breakdown. So far, research on thermoacoustics, especially the flame dynamics, has been performed separately for propagation-stabilized flames and autoignition-stabilized flames. In this paper, we propose an analytical model to predict the response of a composite flame partly stabilized by propagation and partly by autoignition. We leverage a previously developed segmentation method to incorporate both flame types in the same FEM computation. Using the segmentation mechanism, different FTFs are prescribed to the propagation- and autoignition-stabilized flame regions. For the propagation-stabilized HRR regions, a classical $n-\tau-\sigma$ model is used. For the autoignition-stabilized HRR regions, the FTF obtained from a Lagrangian particle tracking based approach is used. Results showed a very good

fit in comparison to forced CFD data. Consequently, the framework can be used to compute longitudinal eigenmode stability predictions of partly autoignition and propagation-stabilized flames and can aid the development of novel emissions-free industrial gas turbine combustors.

Acknowledgements

The research work presented in this manuscript was carried out within the FLEX4H2 project. The FLEX4H2 project is supported by the Clean Hydrogen Partnership and its members European Union, Hydrogen Europe and Hydrogen Europe Research (GA 101101427), and the Swiss Federal Department of Economic Affairs, Education and Research, State Secretariat for Education, Research and Innovation (SERI). Views and opinions expressed are however those of the author(s) only and do not necessarily reflect those of the European Union or any other granting authority. Neither of them is liable for any use that may be made of the information contained therein.

References

[1] United Nations. Paris agreement, 2015.

[2] IEA. World energy outlook 2022, 2022.

[3] Bundesamt für Energie. Energieperspektiven 2050+, 2021.

[4] Expert Group Security of Supply ETH Zurich. Energy security in a net zero emissions future for switzerland, 2023.

[5] Ciani A, Bothien M, Bunkute B et al. Superior fuel and operational flexibility of sequential combustion in Ansaldo Energia gas turbines. *J Glob Power Propuls Soc* 2019; 3: 630–638. DOI:10.33737/jgpps/110717.

[6] Bothien MR, Ciani A, Wood JP et al. Toward decarbonized power generation with gas turbines by using sequential combustion for burning hydrogen. *J Eng Gas Turbines Power* 2019; 141: 121013. DOI:10.1115/1.4045256.

[7] Farhat H and Salvini C. Novel gas turbine challenges to support the clean energy transition. *Energies* 2022; 15. DOI: 10.3390/en15155474.

[8] Goldmeer J, Buck C, Suleiman B et al. Techno-economic analysis of hydrogen and ammonia as low carbon fuels for power generation. In *Proceedings of ASME Turbo Expo 2023*.

[9] Kloess M and Zach K. Bulk electricity storage technologies for load-leveling operation - an economic assessment for the austrian and german power market. *International Journal of Electrical Power and Energy Systems* 2014; 59: 111–122. DOI:10.1016/j.ijepes.2014.02.002.

[10] Bothien MR, Pennell DA, Zajadatz M et al. On key features of the aev burner engine implementation for operational flexibility. Proceedings of ASME Turbo Expo 2013.

[11] Gruber A, Bothien MR, Ciani A et al. Direct numerical simulation of hydrogen combustion at auto-ignitive conditions: Ignition, stability and turbulent reaction-front velocity. *Combustion and Flame* 2021; 229. DOI:10.1016/j.combustflame.2021.02.031.

[12] Casel M and Ghani A. Analysis of the flame dynamics in methane/hydrogen fuel blends at elevated pressures. *Proc Combust Inst* 2023; 39: 4631–4640. DOI:10.1016/j.proci.2022.07.211.

[13] Gruber A, Meyer OHH, Heggset T et al. Numerical investigation of reheat hydrogen flames in the sequential-combustion stage of a heavy-duty gas turbine. In *Proceedings of ASME Turbo Expo 2024 Turbomachinery Technical Conference and Exposition GT2024*.

[14] Nicoud F, Benoit L, Sensiau C et al. Acoustic modes in combustors with complex impedances and multidimensional active flames. *AIAA Journal* 2007; 45: 426–441. DOI: 10.2514/1.24933Ãf.

[15] Laera D, Schuller T, Prieur K et al. Flame describing function analysis of spinning and standing modes in an annular combustor and comparison with experiments. *Combustion and Flame* 2017; 184: 136–152. DOI:10.1016/j.combustflame.2017.05.021.

[16] Campa G and Camporeale S. Eigenmode analysis of the thermoacoustic combustion instabilities using a hybrid technique based on the finite element method and the transfer matrix method. *ADVANCES IN APPLIED ACOUSTICS* 2012; 1: 1–14.

[17] Heinzmann SM, Gopalakrishnan HS, Gant F et al. Development and validation of a framework to predict the linear stability of transverse thermoacoustic modes of a reheat combustor. *Combustion and Flame* 2025; 275: 114010. DOI:https://doi.org/10.1016/j.combustflame.2025.114010. URL `https://www.sciencedirect.com/science/article/pii/S0010218025000483`.

[18] Heinzmann SM, Gopalakrishnan HS, Wood B et al. Linear stability analysis of transversal thermoacoustic modes in reheat combustors. *Proceedings of GT2025 ASME Turbo Expo 2025,GT2025-152879* 2025; .

[19] Silva CF, Nicoud F, Schuller T et al. Combining a helmholtz solver with the flame describing function to assess combustion instability in a premixed swirled combustor. *Combustion and Flame* 2013; 160: 1743–1754. DOI:10.1016/j.combustflame.2013.03.020.

[20] Silva CF, Magri L, Runte T et al. Uncertainty quantification of growth rates of thermoacoustic instability by an adjoint helmholtz solver. *Journal of Engineering for Gas Turbines and Power* 2017; 139. DOI:10.1115/1.4034203.

[21] Crocco L. Aspects of combustion stability in liquid propellant rocket motors part i: Fundamentals. Low frequency instability with monopropellants. *Journal of the American Rocket Society* 1951; 21: 163–178. DOI:10.2514/8.4393.

[22] Schuermans B. *Modeling and control of thermoacoustic instabilities*. PhD Thesis, EPFL, 2003.

[23] Schuermans B, Bellucci V, Guethe F et al. A detailed analysis of thermoacoustic interaction mechanisms in a turbulent premixed flame. In *Proceedings of ASME Turbo Expo 2004 Power for Land, Sea, and Air*.

[24] Noiray N, Bothien M and Schuermans B. Analytical and numerical analysis of staging concepts in annular gas turbines, 2010.

[25] Laurent C, Bauerheim M, Poinsot T et al. A novel modal expansion method for low-order modeling of thermoacoustic instabilities in complex geometries. *Combustion and Flame* 2019; 206: 206. DOI:10.1016/j.combustflame.2019.05.010Ãf.

[26] Bothien MR, Noiray N and Schuermans B. A novel damping device for broadband attenuation of low-frequency combustion pulsations in gas turbines. *J Eng Gas Turbines Power* 2014; 136: 041504. DOI:10.1115/1.4025761.

[27] Heinzmann S, Gopalakrishnan H, Wood B et al. Linear stability analysis of transversal thermoacoustic modes

in reheat combustors. *Journal of Engineering for Gas Turbines and Power* 2025; : 1–19DOI:10.1115/1.4069453. URL https://doi.org/10.1115/1.4069453. https://asmedigitalcollection.asme.org/gasturbinespower/article-pdf/doi/10.1115/1.4069453/7530914/gtp-25-1285.pdf.

[28] Kulkarni R. *Large Eddy Simulation of Autoignition in Turbulent Flows*. PhD Thesis, Technische Universität München, 2013.

[29] Kulkarni R, Bunkute B, Biagioli F et al. Large eddy simulation of alstom's reheat combustor using tabulated chemistry and stochastic fields-combustion model. DOI: 10.1115/GT2014-26053.

[30] Zellhuber M, Bellucci V, Schuermans B et al. Modelling the impact of acoustic pressure waves on auto-ignition flame dynamics. In *Proceedings of the European Combustion Meeting 2011*.

[31] Gant F, Gruber A and Bothien MR. Development and validation study of a 1D analytical model for the response of reheat flames to entropy waves. *Combustion and Flame* 2020; 222: 305–316. DOI:10.1016/j.combustflame.2020.09.005.

[32] Gopalakrishnan HS, Gruber A and Moeck J. Response of auto-ignition-stabilized flames to one-dimensional disturbances: Intrinsic response. *J Eng Gas Turbines Power* 2021; 143: 121011. DOI:10.1115/1.4052058.

[33] Gopalakrishnan HS, Heggset T, Gruber A et al. Prediction of autoignition-stabilized flame dynamics in a backward-facing step reheat combustor configuration. In *Symposium on Thermoacoustics in Combustion: Industry meets Academia (SoTiC 2023)*.

[34] Gopalakrishnan HS, Gruber A and Moeck JP. Computation and prediction of intrinsic thermoacoustic oscillations associated with autoignition fronts. *Combustion and Flame* 2023; 254: 112844. DOI:10.1016/j.combustflame.2023.112844.

[35] ANSYS. Ansys fluent user's guide, 2024. URL http://www.ansys.com.

[36] Brandt M. *Beschreibung der Selbstzündung in turbulenter Strömung unter Einbeziehung ternärer Mischvorgänge*. PhD Thesis, Technische Universität München, 2005. URL https://mediatum.ub.tum.de/601964.

[37] deBruynKops S and Riley J. Large-eddy simulation of a reacting scalar mixing layer with arrhenius chemistry. *Computers Mathematics with Applications* 2003; 46(4): 547–569. DOI:https://doi.org/10.1016/S0898-1221(03)90016-2. URL https://www.sciencedirect.com/science/article/pii/S0898122103900162. Turbulence Modelling and Simulation.

[38] Magnussen B and Hjertager B. On mathematical modeling of turbulent combustion with special emphasis on soot formation and combustion. *Symposium (International) on Combustion* 1977; 16(1): 719–729. DOI:https://doi.org/10.1016/S0082-0784(77)80366-4. URL https://www.sciencedirect.com/science/article/pii/S0082078477803664.

[39] Mechanical and Aerospace Engineering (Combustion Research). Chemical-kinetic mechanisms for combustion applications. http://combustion.ucsd.edu, Accessed 2025. San Diego Mechanism web page, University of California at San Diego.

[40] Weller H, Tabor G, Jasak H et al. A tensorial approach to computational continuum mechanics using object orientated techniques. *Computers in Physics* 1998; 12: 620–631. DOI: 10.1063/1.168744.

[41] Franke F, Bothien M and Sattelmayer T. Flame transfer function measurements of hydrogen-enriched reheat flames. *Combustion and Flame* 2025; 273: 113949. DOI: https://doi.org/10.1016/j.combustflame.2024.113949. URL https://www.sciencedirect.com/science/article/pii/S0010218024006588.

[42] Polifke W and Lawn C. On the low-frequency limit of flame transfer functions. *Combustion and Flame* 2007; 151(3): 437–451. DOI:https://doi.org/10.1016/j.combustflame.2007.07.005. URL https://www.sciencedirect.com/science/article/pii/S0010218007001952.

[43] Rosenkranz JA and Sattelmayer T. Experimental investigation of high frequency flame response on injector coupling in a perfectly premixed multi-jet combustor. *J Eng Gas Turbines Power* 2023; 145. DOI:10.1115/1.4063375.